© Universiti Tun Hussein Onn Malaysia Publisher's Office

IJIE

http://penerbit.uthm.edu.my/ojs/index.php/ijie
ISSN : 2229-838X e-ISSN : 2600-7916

The International Journal of Integrated Engineering

The Effect of Different Reynolds Number On Solid Sphere Using CFD and Its Verification

Mohamad Amirur Rahman Azahar[1], Izuan Amin Ishak[1], Syabillah Sulaiman[1], Norrizam Jaat[1], Abdul Fathul Hakim Zulkifli[1], Safra Liyana Sukiman[2], Kahar Osman[3], Nofrizalidris Darlis[1*]

[1]Department of Mechanical Engineering Technology, Faculty of Engineering Technology,
Universiti Tun Hussein Onn Malaysia, Pagoh Education Hub, 84600, Panchor, Johor, MALAYSIA

[2]Centre for Language Studies,
University Tun Hussein Onn Malaysia (UTHM), Batu Pahat, MALAYSIA

[3]Faculty of Engineering,
Universiti Teknologi Malaysia, MALAYSIA

*Corresponding Author

DOI: https://doi.org/10.30880/ijie.2023.15.01.009
Received 16 June 2021; Accepted 17 October 2021; Available online 28 February 2023

Abstract: Aerodynamic behaviour of an object depends on several factors, namely shape, size and flow conditions. Thus, CFD simulations are an effective engineering tools that allows major contribution to understand the flow conditions around an object. This study aims to analyse the effect of two types of spherical models that are sphere and hemisphere on aerodynamics behaviour for different Reynolds number between 100,000 ≤ Re ≤ 800,000. Geometry models are generated using SolidWorks software and numerical solution is analysed using ANSYS CFX. The numerical results are later compared with experimental data collected from wind tunnel. At the end of the study, the nature flow around spherical models of different Reynolds number are visualized. It is discovered that the flow behaviour around the spherical model changes as the Reynolds number increases. This finding is parallel with past researchers. These forecasts should assist engineers enhance the application of aerodynamic and hydrodynamic design.

Keywords: Aerodynamics, CFD, drag coefficient, wind tunnel

1. Introduction

Aerodynamic analysis, which plays important roles in design and performance of aircraft have been studied since the first development of powered flights (1903) until today [1]. Now, Computational Fluid Dynamics (CFD) has complemented experimental studies, reducing cost in tests and time to generate prototypes [1-3]. Hence, CFD plays a crucial role in replacing wind tunnels in design conditions and modelling turbulent approach for complex problems [4]. Aerodynamic evaluation of larger systems, from automobiles to aircraft, is an important topic that requires considerable commitment and financial investment in today's efficiency-driven environment. If the product's use is racing, where speed is important, or commercial shipping, where the ultimate priority is the productivity of transporting products across the world, wind tunnel tests and CFD simulations should be regarded as an area of serious concern [5].

Previous study on the effect of aerodynamic results generated by CFD simulation and wind tunnel experiment was examined using various models and designs [6,7,16]. Bogos et al. [6] proposed a suitable low Reynolds air foil for unmanned aerial vehicles (UAVs) or a wind turbine blade. Five different models were utilised to test the lowest

*Corresponding author: nofrizal@uthm.edu.my

Reynolds number and SST k-ω turbulence was proven to be the most appropriate model [3]. Muthuvelet et al [7] further annotated numerical simulation airflow for a formula one (F1) vehicle, with spoiler fitted at a rear side of the vehicle at different angles. This vehicle was run at various speeds, from 80 km/h to 120 km/h. The F1 car with a spoiler was analysed using an unstructured polyhedral mesh. The AKN k- turbulence model was utilized, and it was discovered that a lower angle resulted in reduced drag [7].

In the design process, it would be unworkable to analyse various substantial configuration modifications without the use of CFD, especially during the initial stage. In a short time, the capability to achieve results using CFD is characterized by wind tunnel tests that take time to build or modify a model. CFD gives fast solutions, but it is not an irrelevant test for wind tunnels. Though wind tunnel data still play an important role in validating design configurations, with its comprehensive configuration analysis, CFD simulations may go farther and improve the ability to quickly create prototypes. However, basic wind tunnel studies in areas such as flow stability, 3-D boundary layers and flow separation qualities required significantly to validate the CFD results. CFD simulation accuracy can be increased by data validation, and even before entering the wind tunnel, it can simulate results for conceptual design.

The aims of this study to analyse the effect of different geometry shape on aerodynamics behaviour and validated numerical results will be compared with experimental data. Numerical analysis of flow over a geometry is performed using CFD software, ANSYS CFX whilst Aerolab Educational Wind Tunnel (EWT) is used to obtain experimental data. CFD is generally a fluid mechanics branch that uses computer-assisted numerical methods to solve and analysing fluid flow phenomena.

2. Methodology

2.1 Aerodynamic Characteristics

Aerodynamics refers to the research of force and the motion of bodies in air. It has a significant impact on vehicle features such as manoeuvrability, noise, efficiency, and fuel economy [8]. Bernoulli's Theorem is a theory used in different engineering applications to save energy for perfect fluids in steady, streamline, or flow [7]. According to Bernoulli's theorem, the following total is constant for incompressible, friction-free fluid:

$$P + \frac{1}{2}\rho v^2 + \rho g h = \text{constant} \quad (1)$$

where P is the absolute pressure, ρ is the fluid density, v is the velocity of the fluid, h is the height of reference point, and g is the acceleration of gravity. In fluid dynamics, the drag coefficient is a dimensionless variable used to quantify the drag or resistance of an item such as air or water in a fluid system. The drag coefficient is always proportional to a certain area of air [9]. Hence, it is defined as:

$$c_d = \frac{2F_d}{\rho \mu^2 A} \quad (2)$$

Where Fd is drag force, ρ is the fluid density, μ is the flow speed of the object, and A is the reference area. The Reynolds number (Re) would describe the flow patterns in different conditions of fluid flow. Flows are frequently influenced by laminar flow at low Reynolds numbers, whereas flows are frequently turbulent at high Reynolds numbers. Turbulence is created by variances in fluid speed and direction, which can occasionally cross or be directed in the overall flow direction. The Reynolds number is defined as:

$$Re = \frac{\rho u L}{\mu} \quad (3)$$

where Re is the drag force, ρ is the fluid density, u is the flow speed of the object, L is the characteristic linear dimension, and μ is the fluid dynamic viscosity. DC for spherical reference data is roughly 0.4 in the range of Reynolds numbers below the crucial value and reduces to 0.1 above the significance value. When the critical Reynolds number (i.e., the boundary layer separation) is exceeded, a transition occurs on the front face, the boundary layer surrounding the sphere becomes turbulent, and the coefficient of drag rapidly decreases as the boundary layer separation point moves back [10].

2.2 Geometrical Modelling

Table 3.1 indicates the basic dimension of model such as diameter, weight, circumference and length of mounting sting obtained from the measurement process of Aerolab drag model and Aerolab Educational Wind Tunnel Brochure provided in Aerolab official website. The geometry of the Aerolab drag models are generated using SolidWorks 2017 and its numerical solution is run by ANSYS CFX. Figure 1 shows the drawing of sphere and hemisphere models designed in SolidWorks 2017.

Table 1 - Dimension of sphere/hemisphere model

Description	Specification
Diameter	75 mm
Volume	221 cm^3 / 110cm^3
Weight	100 g / 60 g
Length of mounting sting	70 mm

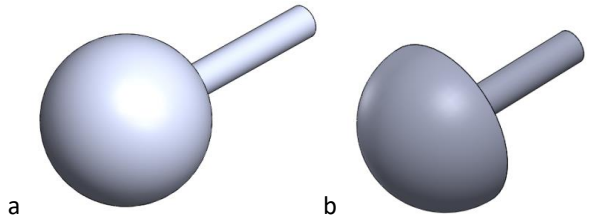

Fig. 1 - Drawing of spherical models (a) sphere model; (b) hemisphere model

2.3 Educational Wind Tunnel

A wind tunnel is a method of studying effects of air flow through solid objects used in aerodynamic research. It comprises of a closed tubular tunnel, which contains an object tested, and flows the air through the object, and a powerful fan system. Wind tunnels can also be categorised according to its operational flow systems and the appropriate dimensional parameters. Table 2 shows the basic dimension of the Aerolab Wind Tunnel such as length, weight, power and airspeed range obtained from Aerolab Educational Wind Tunnel Brochure provided in Aerolab official website. To obtain fully developed flow, the flow is replicated over many rigid spheres in the flow direction of a 610 x 305 x 305 mm test area. Design Modeler was used to construct this test part. SOLIDWORKS 2017 is used to create two sphere models with 75mm and 102mm diameters, as well as a 75mm hemisphere model. These models are imported into ANSYS CFX 19.2 for finite volume discretization of the Navier-Stokes equation. The computer model and boundary conditions are depicted in Figure 3.

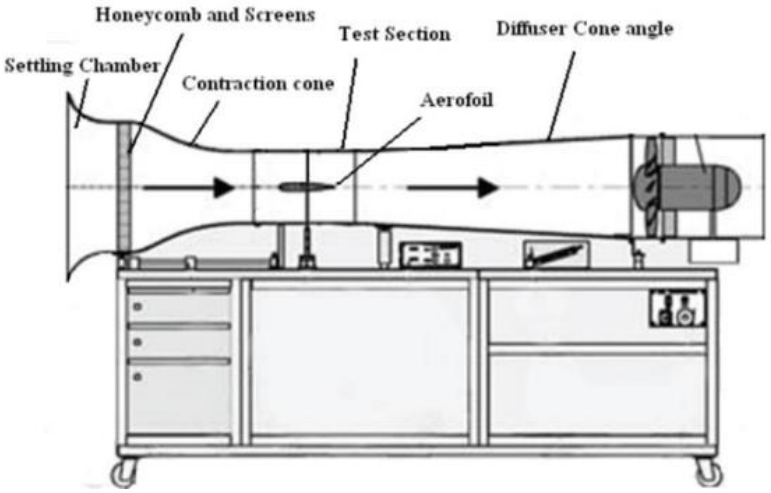

Fig. 2 - Main parts of educational wind tunnel [11]

Table 2 - Specifications of educational wind tunnel [11]

Description	Specification
Length	4.6 m
Width	1.1 m
Height	1.6 m
Weight	272 kg
Power	7.5 KW electric motor
Test Section Dimension	30.5cm x 30.5cm x 61cm
Airspeed Range	4.5 m/s - 65 m/s
Turbulence Level	Less than 0.2 %

2.4 Computational Fluid Dynamics (CFD)

Each computational domain model is constructed as shown in Figure 4 using tetrahedral mesh. Due to its complexity and the need of achieving two points between the fluid domain and wall domain, the tetrahedral mesh was considered. The finest meshing near the spherical configuration is used to achieve the finest result [12,13]. The model is fixed to solid, non-slip surfaces. Air is the working fluid. The outlet opening boundaries are defined to 0 Pa atmospheric pressure, while the inlet boundary is set to a velocity profile minimum of 3m/s to 24m/s, increasing the Reynolds number in the turbulent flow range of 100,000 to 800,000. As the flow is assumed to be totally turbulent, realisable k- turbulence is employed in the study to attain greater flow performance with separation.

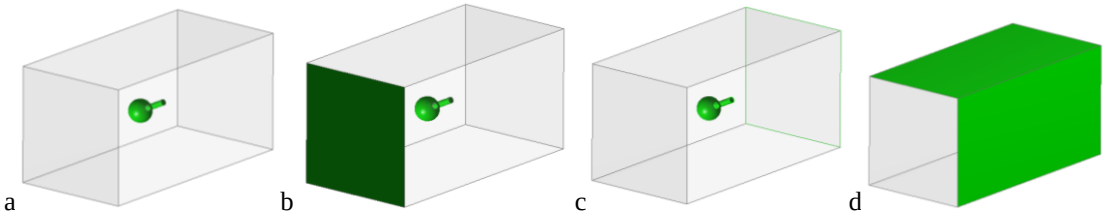

Fig. 3 - The boundary conditions (a) model wall; (b) velocity inlet; (c) pressure outlet; (d) wall

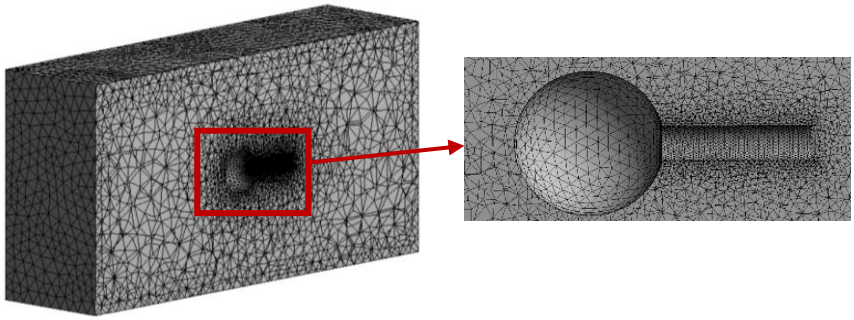

Fig. 4 - Mesh of computational domain

3. Results

3.1 Grid Independence Test

Grid Independence is a term used to describe the improved results obtained by using smaller cell sizes for subsequent calculations [18,19]. As the mesh grows finer, a computation should approach the same findings, implying grid independence. Figure 5 depicts the velocity distribution for one of the sphere models, a 75mm-diameter sphere with a variable number of nodes. This model was chosen as the sphere's benchmark because it exhibits consistent low velocity and normal pressure when compared to other models. As a result, the mesh sizing is raised approximately from 150,000 to 250,000 nodes to see substantial changes in the velocity distribution. The Grid Independence Test reveals no significant changes in the velocity distribution for nodes ranging from 200,000 to 250,000, with an average relative inaccuracy of less than 1%. As a result, following simulations are limited to 200,000 nodes or greater. Because of the grid independence of this model, the cell size should be lowered in stages to minimise discretization mistakes, and the mesh configuration used for the other models should be the same.

3.2 Drag Coefficient

Drag force is the component of resultant pressure and shear forces acting in the flow direction. The drag coefficient is calculated from the drag force, and various free stream velocity values ranging from 100,000 to 800,000 are tested using CFD simulation. Figures 6 and 7 depict this drag coefficient. Figure 6 depicts a comparison of numerical and experimental data for flow around a 75mm sphere in terms of integral features as a function of drag coefficient vs Reynolds number. Each approach yields a maximum difference of 40%, although for Reynolds numbers more than 600,000, the difference is less than 10%. The average drag coefficient for experimental results is 0.2413 whilst for numerical results is 0.2009 and the percentage difference for each result is 16%. It is evident that the value of the drag coefficient exhibits converging pattern as the value of the Reynolds number increases.

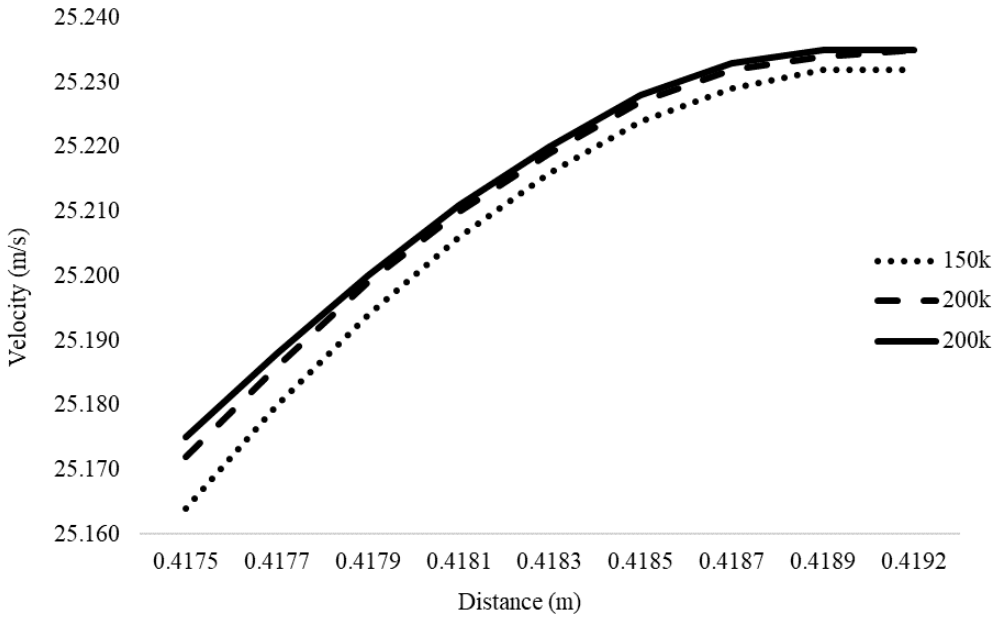

Fig. 5 - Grid independence test result with three different nodes number

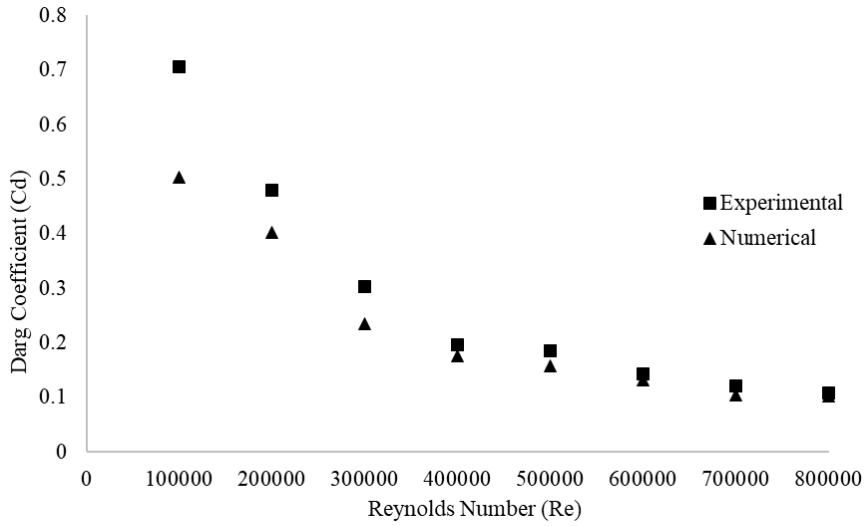

Fig. 6 - Drag coefficient versus Reynolds number for 7.5mm sphere

For 7.5mm hemisphere, comparison between both methods display maximum difference of 60% and this difference is lesser than 10% when the Reynolds number is over 700,000, see Figure 7. The average drag coefficient for experimental results is 0.2497 whereas for numerical results, it is 0.1962 with the percentage difference of 21% for each result. These differences are probably due to inadequacy of domain geometry when meshing is applied [20]. More importantly, it is the result of a physical model insufficiency, which does not enable full modelling of transition processes in the drag coefficient's abrupt decrease zone. When the flow in the boundary layer becomes turbulent, the drag coefficient lowers as the Reynolds number increases, allowing a separation point to travel further away from the rear body, lowering wake size and pressure drag magnitude. These findings are consistent with prior research, which found that the annotated drag coefficient falls as the Reynolds number increases [14,16].

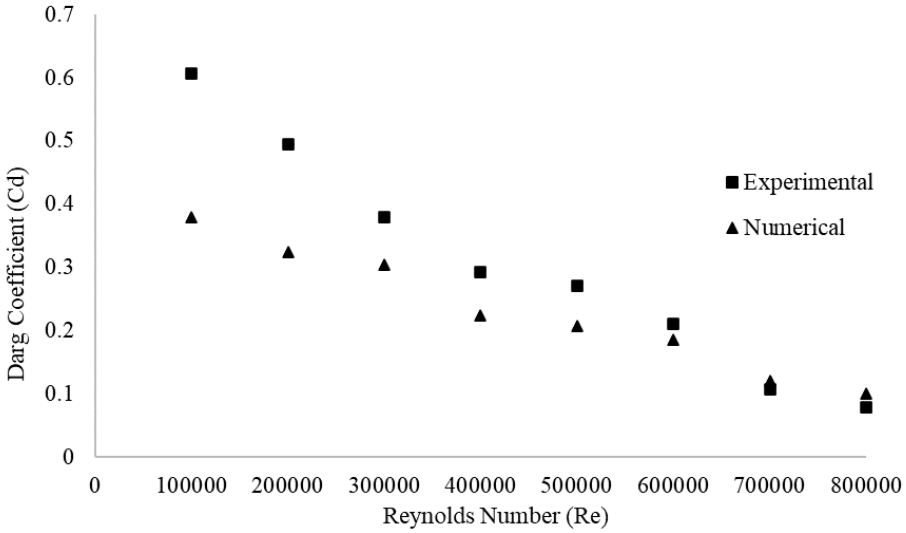

Fig. 7 - Drag coefficient versus Reynolds number for 7.5mm hemisphere

3.3 Velocity Streamline

The characteristics of the flow field and its structure, such as the stagnation point and recirculation zone, are seen and investigated using velocity streamlines, as illustrated in Figure 8. A stagnation point is a place in a flow field where the fluid's local velocity is zero, whereas a recirculation zone is a particular circumstance in which the flow splits from the body of the barrier and produces a low-pressure area. The velocity distribution profiles of airflow around spherical model are illustrated in Figure 9 and Figure 10 with an enlarged view of the test section area. As it can be seen in both figures, the magnitude flow velocity changes in all areas. These figures show the velocity streamlines around the models for Reynolds number ranged from 100,000 to 800,000, respectively.

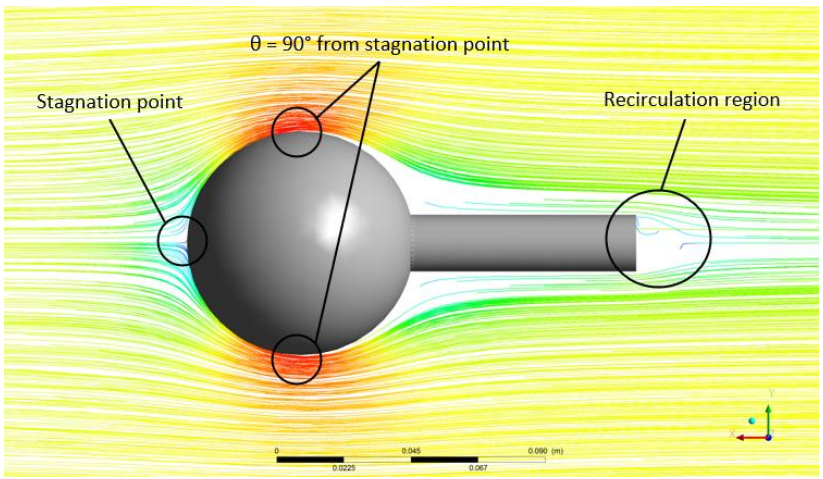

Fig. 8 - Velocity streamlines with some references point

Figure 9 depicts the streamlines at various Reynolds numbers, indicating that this flow region is regarded a steady-state wake [15]. When fluid flows past wall tubes, it decelerates to the tube's surface, where viscous processes generate a thin layer known as the boundary layer. The tube's surface is coupled to the flow until the wake is generated, which is visible at the back of the tube where some fluid is flowing backward against the main flow. The impact causes the flow to split into the top and lower regions of the model, causing a stagnation point to emerge at the centre point of the spherical front surface. The maximum velocity occurs at $\theta = 90°$ from stagnation point. The speed is at minimum or zero, near $\theta = 180°$. Here the circulation usually occurs. A very weak recirculation zone has been connected to the rear of the sphere. As the value of the Reynolds numbers rises, the Wake grows broader and longer, and the point of attachment on the sphere advances forward.

In the case of the hemisphere, the velocity distribution around the models is shown in Figure 10. From the figure, massive recirculation region is formed in the wake area. There is an apparent instability in all tested Reynolds numbers for wake at the back of the hemisphere. This region is known as the laminar flow. The graphic shows that when the

Reynolds number grows, a lengthy period of oscillation increases, yet the sphere remains connected to the wake. The outer flow over this region is laminar and will remain so. In terms of vehicle aerodynamics, the recirculation zone is responsible for the majority of the aerodynamic drag difficulties. Starting with this flow pattern, viscous effects or viscous drag have a minor impact in the drag coefficient value. When a point near the surface of the sphere begins to diverge or fall to the minimal flow, flow separation happens. When the shear stress at the wall is zero, the separation point occurs. It demonstrates that when the Reynolds number grows, flow separation happens earlier. These findings agree with past researchers [14,17]. This is because as the velocity rises, the flow has more difficulty attaching to the sphere. When the Reynolds number grows, the inertia effects become more important than the viscous effect, and the flow separation separates from its wall more quickly.

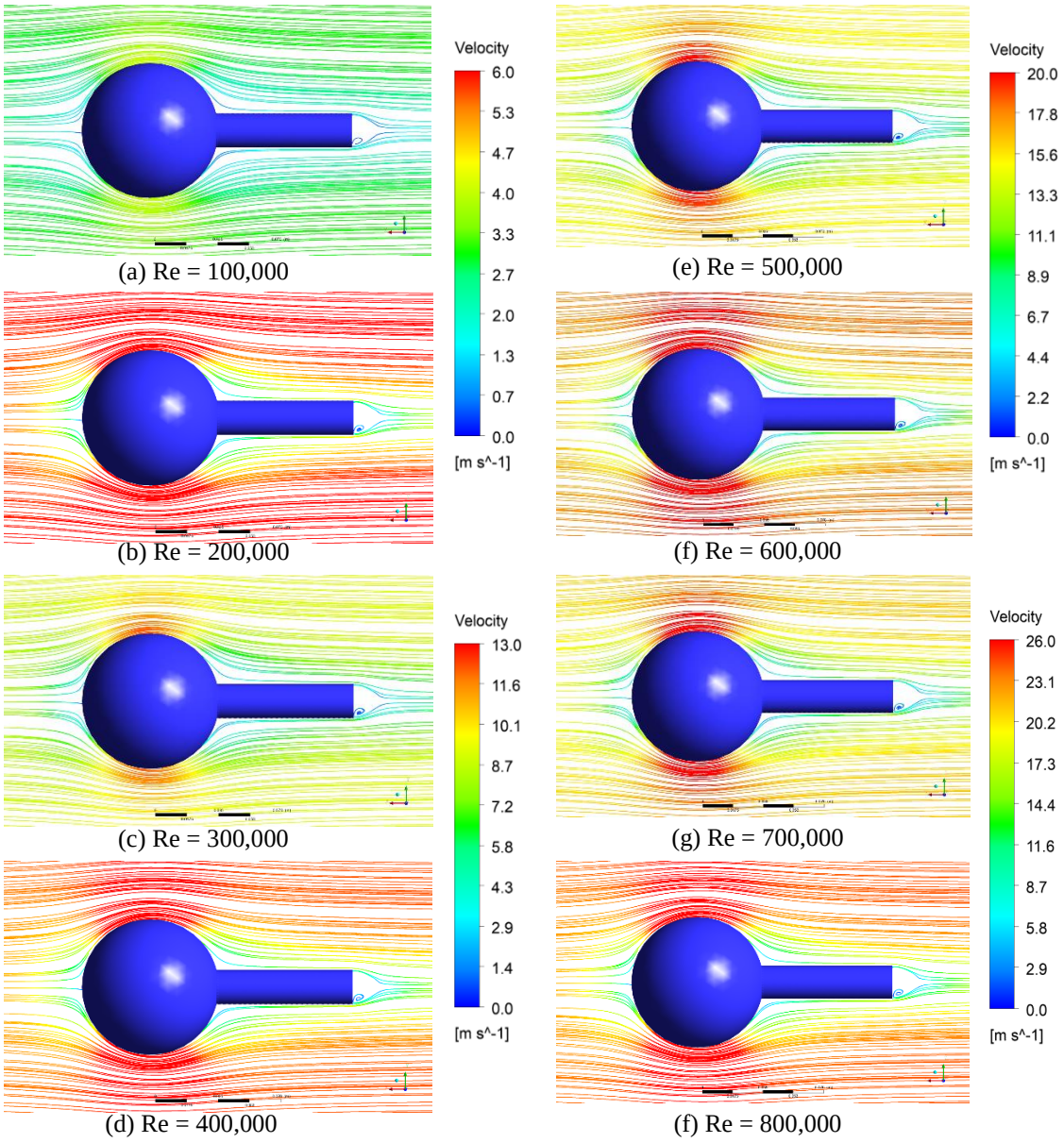

Fig. 9 - Side view of velocity streamlines around 75mm-diameter sphere

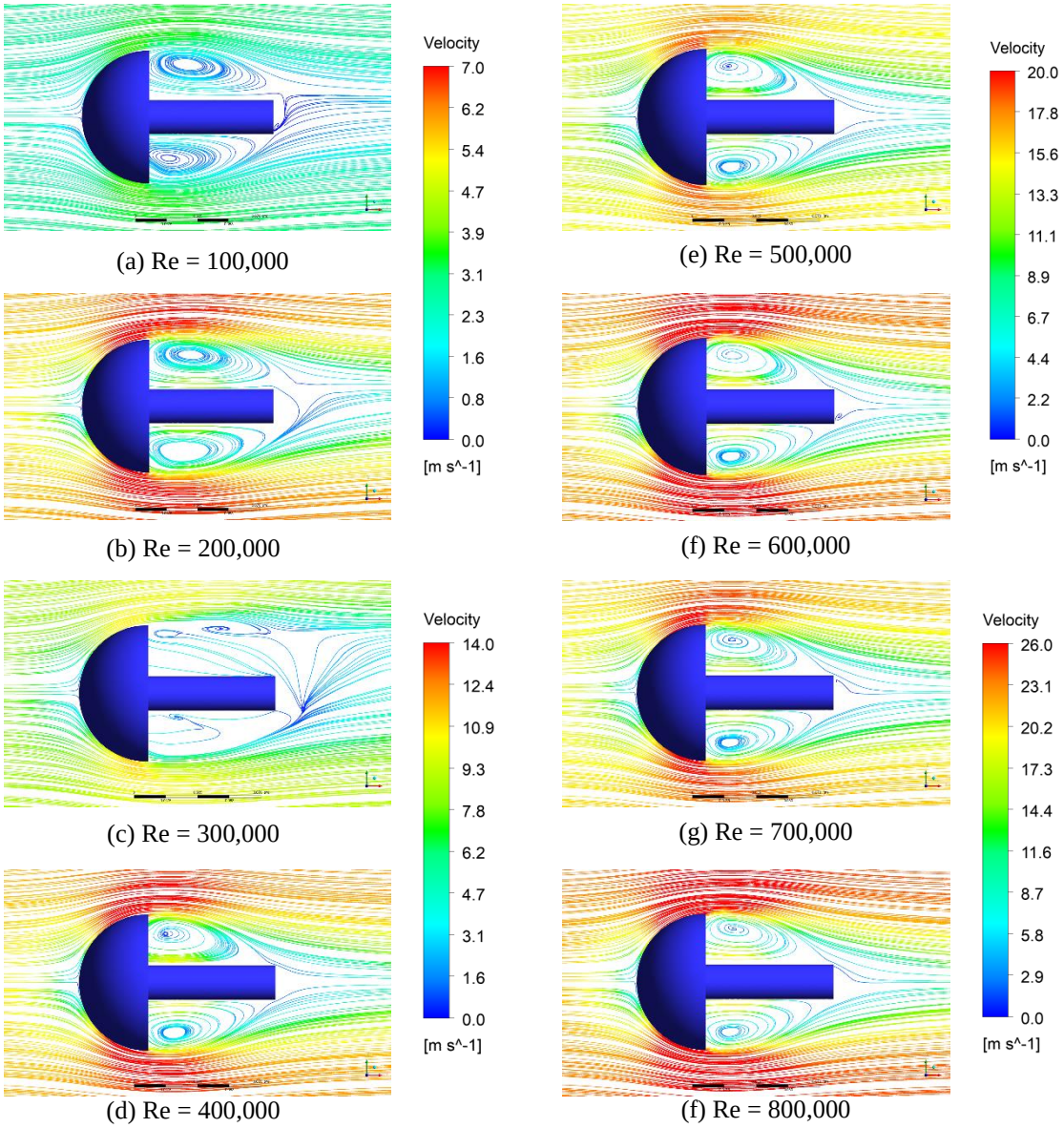

Fig. 10 - Side view of velocity streamlines around 75mm-diameter hemisphere

3.4 Pressure Distribution On the Object Surface

Fluid particles on the midplane collide with the sphere at the stagnation point, causing the fluid to come to a full halt and raising the pressure at that point. It is discovered that it is the maximum point for all Reynolds numbers (100,000 – 800,000). Figure 11 depicts a high-pressure zone formed at the frontal sphere surface as a result of the direct impact of oncoming flow. As explained earlier, this is where the stagnation point occurs with zero velocity streamline. The flow is separated instantly after the impact. This led to low-pressure region on the sphere's top surface as the flow accelerates. On the other hand, the pressure distribution in the middle of the model becomes consistent due to less intense flow. However, there is a pressure differences in the middle of the sphere and the hemisphere areas since the recirculation region is formed in the middle of hemisphere as shown in Figure 11 through the indication of different colours of contour region for sphere (i.e., yellow) and hemisphere (i.e., blue). Meanwhile, Figure 12 shows the side view of pressure contour taken from the sphere model's centreline plane. High-pressure region is evident near the direct impact of the flow on the sphere model's frontal area and the formation of vortices indicated by the low-pressure region's occurs in the middle of the models. Figure 12 (b) lucidly shows the massive area of low-pressure region occurs at the wake, through the representation of recirculation region formed in the hemisphere model.

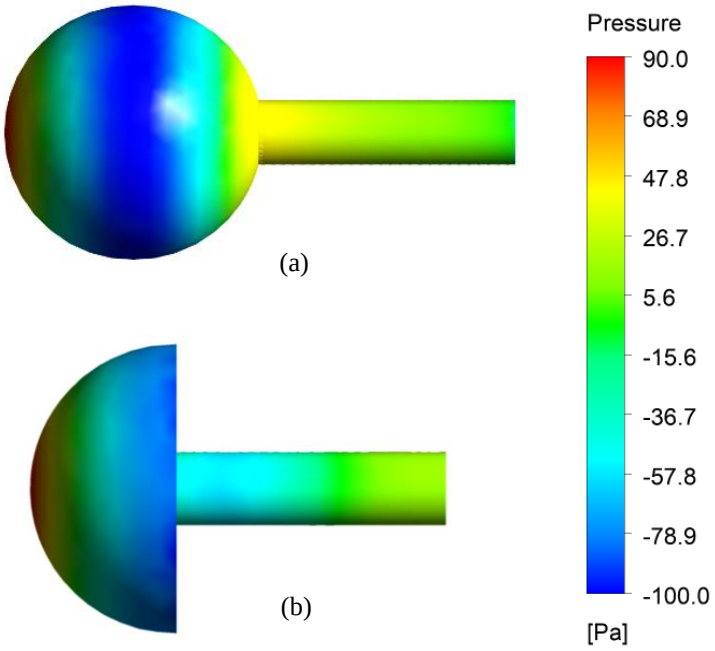

Fig. 11 - The pressure contour around (a) sphere; (b) hemisphere at 400,000 Reynolds number

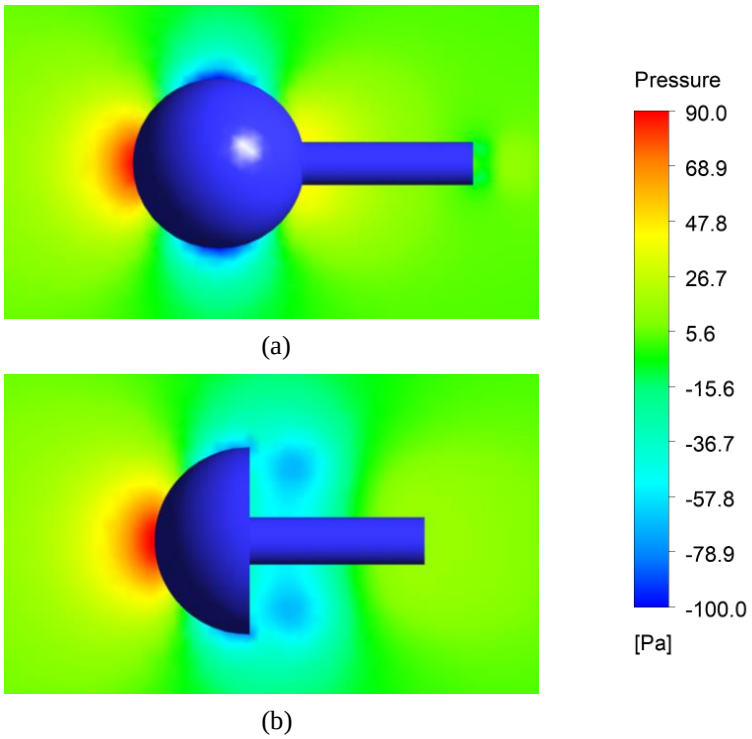

Fig. 12 - The pressure contour around (a) sphere; (b) hemisphere at 400,000 Reynolds number

4. Conclusions

In conclusion, the nature of flow around spherical models for different Reynolds number is visualized. Computational fluid dynamics (CFD) analysis is performed on different spherical models using ANSYS CFX software to analyse aerodynamic performances of drag coefficient, velocity streamline and pressure distribution. In this work, the drag coefficient is compared between experimental and numerical data. The results show that when the Reynolds number grows, the flow behaviour around the spherical model changes. According to the graph's patterns, the Reynolds number rises as the drag coefficient falls. At Re=100,000, the drag coefficient for sphere (cd=0.5) is higher than hemisphere (cd=0.38) since the recirculation region is formed in the middle of hemisphere. In terms of aerodynamics, it

can be said that the recirculation region causes aerodynamic drag issues. These forecasts should assist engineers enhance the application of aerodynamic and hydrodynamic design.

Acknowledgement

This research is supported by Ministry of Education (MOE) through Fundamental Research Grant Scheme (FRGS/1/2020/TK02/UTHM/03/4). The author would like to thank Faculty of Engineering Technology, Universiti Tun Hussein Onn Malaysia for providing feasible research facilities for this study.

References

[1] Aravind Seeni, Parvathy Rajendran, and Hussin Mamat, "A CFD Mesh Independent Solution Technique for Low Reynolds Number Propeller," CFD Letters 11, no. 10 (2019): 15–30.
[2] Abdul Aabid et al., "Cfd Analysis of Splitter Plate on Bluff Body," CFD Letters 11, no. 11 (2019): 25–38.
[3] Samuel Merryisha and Parvathy Rajendran, "Experimental and Cfd Analysis of Surface Modifiers on Aircraft Wing: A Review," CFD Letters 11, no. 10 (2019): 46–56.
[4] Mujeeb R Malik and Dennis M Bushnell, "Role of Computational Fluid Dynamics and Wind Tunnels in Aeronautics R & D," Nasa/Tp-2012-217602, no. September (2012): 1–62.
[5] Peter N Doval and Ilya V Avdeev, "Investigation of Riding Position Effects on Time-Trial Bicycle Drag Coefficient at Different Yaw Angles," November 9, 2012.
[6] Bogos, Stefan, Alexandru Dumitrache, and Florin Frunzulica. 2015. "Turbulence Models in CFD Simulation of Low-Reynolds Number Airfoils Flow." In AIP Conference Proceedings. Vol. 1648. American Institute of Physics Inc.
[7] A Muthuvel, N Prakash, and J Godwin John, "Numerical Simulation of Drag Reduction in Formula One Cars," International Journal of Engineering Research and Applications, no. March (2014): 2248–9622,
[8] Redzuan Ahmad, "Develop Drag Estimation on Hybrid Electric Vehicle (Hev) Model Using Computational Fluid Dynamics (CFD)," Journal of Chemical Information and Modeling 53, no. 9 (2013): 1689–99.
[9] "Drag Coefficient." Wikipedia. Wikimedia Foundation, January 24, 2021.
[10] Anderson, John. D, Introduction to Flight, McGraw-Hill Book Company, New York, USA, 2005.
[11] Louis Cattafesta, Chris Bahr, and Jose Mathew, "Fundamentals of Wind-Tunnel Design," Encyclopedia of Aerospace Engineering, no. December (2010).
[12] Wan Mohamad Aiman Wan Yahaya et al., "The Evaluation of Drag and Lift Force of Groove Cylinder in Wind Tunnel," Journal of Advanced Research in Fluid Mechanics and Thermal Sciences 68, no. 2 (2020): 41–50,
[13] Che Mohammad Hafizal Muzammil Che Seman et al., "Comparison of Hemodynamic Performances between Commercial Available Stents Design on Stenosed Femoropopliteal Artery," CFD Letters 12, no. 7 (2020): 17–25,
[14] Azmahani Sadikin et al., "Numerical Study of Flow Past a Solid Sphere at Moderate Reynolds Number," Applied Mechanics and Materials 660 (2014): 674–78.
[15] Low Reynolds et al., "Particles , Bubbles & Drops : Their Motion , Heat And Mass Transfer , 2006 , 410 Pages , E . E. Michaelides , 9812566473 , 9789812566478 , World Scientific Publ ., 2006" 2 (2012)
[16] Vojtěch Spálenský and Dalibor Rozehnal, "CFD Simulation of Dimpled Sphere and Its Wind Tunnel Verification," MATEC Web of Conferences 107 (2017).
[17] Azmahani Sadikin et al., "Numerical Study of Flow Past a Solid Sphere at Moderate Reynolds Number," Applied Mechanics and Materials 660 (2014): 674–78.
[18] Muhammad Syahmi Abdul Hakim et al., "The Effects of Reynolds Number on Flow Separation of Naca Aerofoil," Journal of Advanced Research in Fluid Mechanics and Thermal Sciences 47, no. 1 (2018): 56–68.
[19] Seyed Reza Jafari Gahraz, Tholudin Mat Lazim, and Masoud Darbandi, "Wind Tunnel Study of the Effect Zigzag Tape on Aerodynamics Performance of a Wind Turbine Airfoil," Journal of Advanced Research in Fluid Mechanics and Thermal Sciences 41, no. 1 (2018): 1–9.
[20] Nadeem Ahmed Sheikh and Shehryar Manzoor, "Numerical Simulation of Phase Map Shift of Vibrating Cylinder at Low Reynolds Number," CFD Letters 5, no. 3 (2013): 97–107.